Mass enhancement and metal-nonmetal transition driven by *d-f* hybridization in perovskite $La_{1-x}Pr_xCuO_3$

H. Takahashi [1,2] M. Ito,[3] J. Fujioka [4] M. Ochi [5,6] S. Sakai [7] R. Arita [3,7]
H. Sagayama,[8] Y. Yamasaki [9] and S. Ishiwata [1,2]

[1]*Division of Materials Physics and Center for Spintronics Research Network (CSRN), Graduate School of Engineering Science, Osaka University, Osaka 560-8531, Japan*
[2]*Spintronics Research Network Division, Institute for Open and Transdisciplinary Research Initiatives, Osaka University, Yamadaoka 2-1, Suita, Osaka 565-0871, Japan*
[3]*Department of Applied Physics, University of Tokyo, Bunkyo-ku, Tokyo 113-8656, Japan*
[4]*Department of Materials Science, University of Tsukuba, 1-1-1 Tennodai, Tsukuba, Ibaraki 305-8573, Japan*
[5]*Department of Physics, Osaka University, Machikaneyama-cho, Toyonaka, Osaka 560-0043, Japan*
[6]*Forefront Research Center, Osaka University, Machikaneyama-cho, Toyonaka, Osaka 560-0043, Japan*
[7]*RIKEN Center for Emergent Matter Science, 2-1 Hirosawa, Wako 351-0198, Japan*
[8]*Institute of Materials Structure Science (IMSS), High Energy Accelerator Research Organization (KEK), Tsukuba, Ibaraki 305-0801, Japan*
[9]*National Institute for Materials Science (NIMS), Tsukuba, Ibaraki 305-0047, Japan*

(Received 12 November 2023; revised 30 January 2025; accepted 31 January 2025; published 28 February 2025)

We report a large electron-mass enhancement and metal-to-nonmetal transition upon Pr doping in perovskite-type $La_{1-x}Pr_xCuO_3$. With increasing the Pr content x around 0.6, the $LaCuO_3$-type three-dimensional structure with trivalent Cu ions changes to a quasi-one-dimensional structure with nearly divalent Cu ions, which accompanies significant changes in the electronic properties. Based on the resistivity, optical conductivity, specific heat measurements, and first-principles calculations, we discuss the formation of a nearly localized nonmetallic state stabilized by the hybridization between Cu $3d$, O $2p$, and Pr $4f$ orbitals in the quasi-one-dimensional lattice. The present perovskite-type cuprates offer a unique opportunity to explore novel quantum phases of correlated electrons in a low-dimensional lattice where the spin/charge/orbital degrees of freedom of A- and B-site ions are entangled.

DOI: 10.1103/PhysRevB.111.085153

I. INTRODUCTION

Perovskite-type transition-metal oxides ABO_3 have been extensively explored as functional materials showing a rich variety of magnetic and electronic properties [1]. The rich electronic functions derive typically from the strongly correlated d electrons in the three-dimensional B-O lattice. This is exemplified by $AMnO_3$ with a giant magnetoelectric effect [2,3] and $ANiO_3$ with a metal-insulator transition [4,5], in which the A site is occupied by the trivalent rare-earth ions. On the other hand, it has been demonstrated that the charge and orbital degrees of freedom of A-site ions can be involved in the electronic properties of perovskite oxides when the B site is occupied by late $3d$ transition-metal ions with high valence state. For instance, (La, Bi)NiO_3 and (La, Sr)$Cu_3Fe_4O_{12}$ show gigantic negative thermal expansion due to the intersite charge transfer between Bi and Ni, and Cu and Fe, respectively [6–11].

Although considerable efforts have been made to study perovskite oxides with various $3d$-transition-metal ions, less is known about the perovskite-type cuprates $ACuO_3$, which can be regarded as the three-dimensional counterparts of the high-T_c cuprates with layered structure. The scarcity of perovskite-type $ACuO_3$ presumably reflects the fact that $ACuO_3$ with unusually high-valence Cu^{3+} ions is typically difficult to obtain, while oxygen-deficient perovskites $YBa_2Cu_3O_{6+x}$ with superconducting CuO_2 planes have been extensively synthesized at ambient pressure [12]. So far, perovskite-type cuprates without oxygen deficiency have been reported for $LaCuO_3$ and its substitution of La by Nd [13–18]. While $La_{1-x}Nd_xCuO_3$ shows an indication of the mass enhancement with increasing x up to 0.6, the system keeps the rhombohedral structure and the metallic behavior down to the lowest temperature [16]. It is presumable that the introduction of magnetic rare-earth ions into the A site of $ACuO_3$ provides novel quantum phases inherent to the intersite charge transfer and the d-f hybridization.

Here we discover the A-site-dependent large mass enhancement and metal-nonmetal transition in perovskite-type cuprates, $La_{1-x}Pr_xCuO_3$, which can be associated with the intersite charge transfer, $A^{3+}Cu^{3+}O_3 \rightarrow A^{(4-\delta)+}Cu^{(2+\delta)+}O_3$. The A-site-dependent transition accompanies significant changes in both crystalline and electronic structures as the three-dimensional rhombohedral structure in a metallic state ($x < 0.6$) to the quasi-one-dimensional orthorhombic structure in a conductive but nonmetallic state ($x > 0.6$). The emergence of the nonmetallic state in $La_{1-x}Pr_xCuO_3$ is discussed in terms of a strong coupling between the $4f$ electrons of $Pr^{3+/4+}$ ion and the $3d$ electrons of $Cu^{2+/3+}$ ion.

 ©2025 American Physical Society

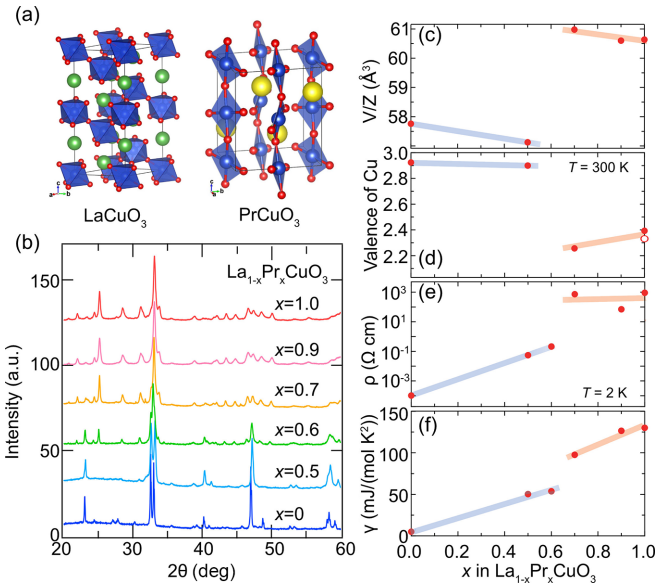

FIG. 1. (a) Crystal structure of $LaCuO_3$ and $PrCuO_3$ [21]. (b) Powder x-ray diffraction patterns of $La_{1-x}Pr_xCuO_3$ taken at room temperature. (c) Normalized unit-cell volume V/Z, where Z denotes the number of formula units per unit cell. (d) Valence of the Cu ion estimated by bond valence sum (filled circles) and x-ray absorption spectra (open circles) [19]. (e) Resistivity at 2 K, and (f) electronic specific heat coefficient γ plotted as a function of x. The blue and red lines correspond to the phases with rhombohedral (R-3c) and orthorhombic ($Pbnm$) symmetry, respectively.

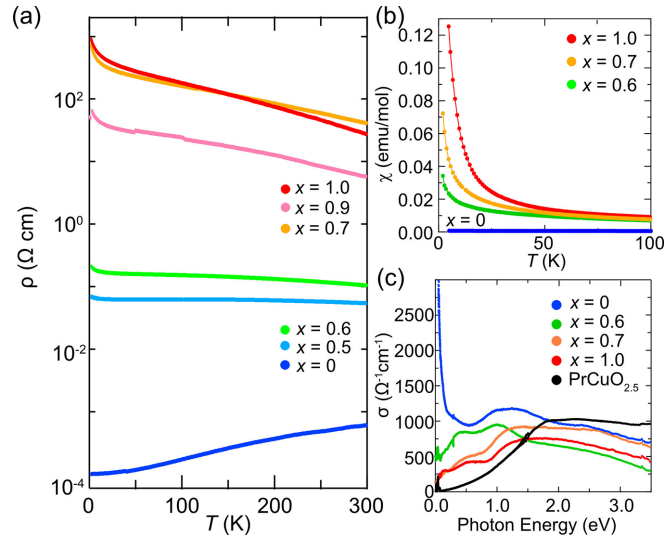

FIG. 2. (a) Temperature dependence of resistivity and (b) magnetic susceptibility for $La_{1-x}Pr_xCuO_3$ with selected compositions. (c) Optical conductivity spectra at room temperature. The spectra of an oxygen-deficient perovskite $PrCuO_{2.5}$ with insulating behavior is shown as a reference.

II. EXPERIMENTAL RESULTS

Polycrystalline samples of $La_{1-x}Pr_xCuO_3$ were prepared as described in the previous report for $PrCuO_3$ [19] (for detailed experimental and theoretical methods, see the Supplemental Material (SM) [20]). Figure 1(b) shows the powder x-ray diffraction (XRD) patterns of $La_{1-x}Pr_xCuO_3$ with selected compositions of $x = 0$, 0.5, 0.6, 0.7, 0.9, and 1.0, indicating the emergence of the A-site-dependent structural transition around $x = 0.6$. The diffraction patterns were indexed with a rhombohedral (R-3c) unit cell for $x = 0$ and 0.5 and orthorhombic ($Pbnm$) unit cell for $x = 0.7$, 0.9, and 1.0. The diffraction pattern of $x = 0.6$ contains the peaks of both structures, implying that this composition is located near the first-order structural phase boundary between them, as shown in Fig. S1 (see SM [20]).

For the selected compounds ($x = 0$, 0.5, 0.7, 1), the crystal structure was refined by the Rietveld analysis for the x-ray diffraction data as shown in Fig. S2 (see SM [20]). Figure 1(c) shows the variation of the unit-cell volume divided by Z, the number of formula units per unit cell, as a function of the Pr content x. In the rhombohedral phase with x less than 0.6, the unit-cell volume decreases monotonically with increasing x, reflecting the decrease in the averaged ionic radius of the A-site ion. As x exceeds 0.6, the rhombohedral structure is replaced by the highly distorted $PrCuO_3$-type structure, accompanying a jump in the unit-cell volume by 7%. Considering the fact that the unit-cell volume of perovskite oxides is strongly affected by the B-O bond length, such a huge volume increase upon the structural change implies the sudden decrease in the valence of the Cu ion as a consequence of the intersite charge transfer. This conjecture is confirmed by the bond-valence-sum (BVS) calculation for Cu in $La_{1-x}Pr_xCuO_3$, as shown in Fig. 1(d). The estimated Cu valence in the composition with x below 0.6 is close to +3, whereas that for x above 0.6 is in the range of +2.2 to +2.4. The nearly divalent nature of Cu ions is consistent with the cooperative Jahn-Teller distortion of the CuO_6 octahedra, which lifts the degeneracy of the e_g orbitals. This result has been supported also by the x-ray absorption near edge structure (XANES) measurements around the Cu K edge [19], whereas the intersite charge transfer with the increment of Pr content in $La_{1-x}Pr_xCuO_3$ reminds us that in $Bi_{1-x}La_xNiO_3$ with the increment of Bi content [9], there exists a distinct difference between them, reflecting the presence of spin and orbital degrees of freedom in the A site of $La_{1-x}Pr_xCuO_3$.

The electronic state of $La_{1-x}Pr_xCuO_3$ changes significantly upon the A-site-dependent structural transition around $x = 0.6$. Figure 2(a) shows the temperature dependence of the electrical resistivity for $La_{1-x}Pr_xCuO_3$. Pr doping on $LaCuO_3$ increases the absolute value of electrical resistivity, and the resistivity at 2 K increases by an order of 3 upon the structural transition between $x = 0.6$ and 0.7, as shown in Fig. 1(e). $La_{1-x}Pr_xCuO_3$ with x larger than 0.6 shows nonmetallic temperature dependence, implying that the charge carriers are in an incoherent state. The significant enhancement of resistivity associated with the structural transition to the quasi-one-dimensional structure presumably suggests the formation of incoherent bands near the Fermi energy, and also the fact that the crystal structure is highly anisotropic for $x > 0.6$ and the sample is polycrystalline, making the resistivity susceptible to scattering at grain boundaries. The x-dependent change in the electronic state of $La_{1-x}Pr_xCuO_3$ can be found in the optical conductivity. The photon energy dependence of optical-conductivity spectra is shown in Fig. 2(c). A clear Drude-like peak is observed below 0.2 eV

TABLE I. Parameters obtained by the Curie-Weiss fitting for $La_{1-x}Pr_xCuO_3$.

	$x = 0.6$	$x = 0.7$	$x = 1.0$
$P_{\rm eff}$ (μ_B)	3.44	3.42	2.68
θ (K)	−54.3	−55.0	−34.9
χ_0 (emu/mol)	7.8×10^{-4}	4.2×10^{-4}	1.2×10^{-3}

for $x = 0$, which is almost absent for $x > 0.6$. However, in contrast to the Mott insulator of $PrCuO_{2.5}$, which has an energy gap of ~ 0.5 eV, a finite intensity is observed at low energies down to 0 eV for $x > 0.6$. This is consistent with the fact that the electrical resistivity of $PrCuO_{2.5}$ is three orders of magnitude larger than that of $PrCuO_3$ at room temperature, as shown in Fig. S3 (see SM [20]). The several humplike structures below 2 eV can be ascribed to $d - d$ transitions inherent to the heavily distorted CuO_6 octahedra. These results indicate that the compounds with $x > 0.6$ have incoherent bands near the Fermi energy, which is consistent with the nonmetallic temperature dependence of the resistivity.

Figure 2(b) exhibits the temperature dependence of the magnetic susceptibility measured under a magnetic field of 0.1 T in a field-cooling run for $x = 0$, 0.6, 0.7, and 1.0 (the magnetic susceptibility of $LaCuO_3$ was taken from Ref. [22]). For $x > 0.6$, the Curie-Weiss-like behavior is observed above about 50 K. The effective Bohr magnetons number $P_{\rm eff}$ was evaluated by the Curie-Weiss law fitting between 100 and 300 K with the formula $M/H = x\, C_{\rm w}/(T - \theta) + \chi_0$ as shown in Fig. S4 (see SM [20]), where $C_{\rm w}$, θ, and χ_0 are the Curie constant, Weiss temperature, and temperature-independent background contributions, respectively, mainly from Pauli paramagnetism. The $P_{\rm eff}$ decreases from 3.44 to 2.68 μ_B/Pr with a change in x from 0.6 to 1.0 (all data are listed in Table I), suggesting that the valence of Pr tends to increase from +3 (theoretical value of $P_{\rm eff} = 3.58\,\mu_B$/Pr) to +4 ($P_{\rm eff} = 2.54\,\mu_B$/Pr). Here, we assume that the localized moment of Pr ions dominates the Curie-Weiss behavior. The x-dependent change in $P_{\rm eff}$ is consistent with the change in the valence of Pr ions expected from the BVS calculations (Table S5 in Supplemental Material shows the BVS of the La/Pr site, where the estimated La/Pr valence in the composition with x below 0.6 is close to +3 and that for x above 0.6 is close to +4 [20]). Whereas the Weiss temperature is negatively as large as −35 K and −55 K, $La_{1-x}Pr_xCuO_3$ exhibits no magnetic transition down to 2 K. This result implies that the magnetic Pr sublattice becomes effectively one dimensional, given that the magnetic interactions between Pr ions are mediated by the Cu-O sublattice.

To gain further insight into the electronic states, we measured the temperature dependence of the specific heat for selected compositions. The specific heat also depends on the Pr content x, as shown in Fig. 3(a) without offset. $LaCuO_3$ exhibits nonmagnetic metallic behavior with a small electronic specific heat coefficient γ ($\sim$5.0 mJ/mol K^2). As x increases above 0.7, C/T shows a substantial upturn at low temperatures, as observed in oxides with Pr^{4+} ions. This upturn of C/T implies the Schottky anomaly of Kramers doublet for Pr^{4+} ions. To confirm this presumption, we evaluate the entropy in $PrCuO_3$ by subtracting the C/T of $LaCuO_3$, which can be

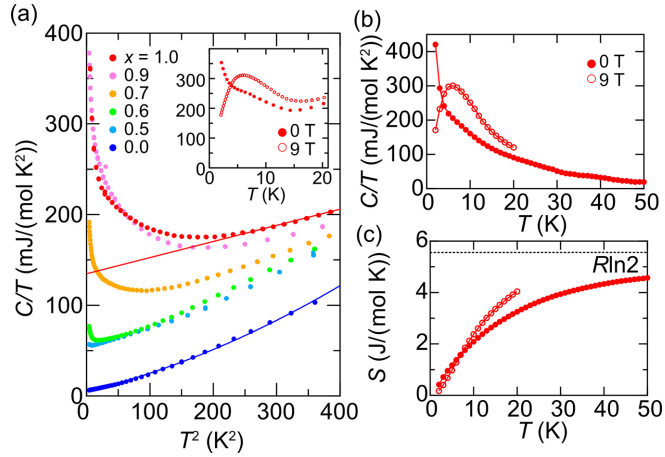

FIG. 3. (a) Specific heat divided by temperature C/T as a function of T^2. The blue and red solid lines correspond to the fits of $C/T = \gamma + \beta T^2 + \alpha T^4$ and $\gamma + \beta T^2$, respectively; the first term is the electronic contribution, and the second and the third are from the lattice [22]. The inset shows T dependence of C/T of $PrCuO_3$ ($x = 1$) under magnetic fields of 0 T and 9 T. (b) Temperature dependence of background-subtracted C/T and (c) entropy for $PrCuO_3$ measured at 0 T and 9 T. The data of $LaCuO_3$ were adopted as each background.

regarded as a background mainly from the lattice contribution, from that of $PrCuO_3$, as shown in Figs. 3(b) and 3(c) (the detailed analysis is shown in Fig. S5). The entropies estimated from the background-subtracted C/T are found to approach $R\ln 2$, supporting the presence of a high percentage of Pr^{4+} ions with a Kramers ground-state doublet in $PrCuO_3$. The temperature dependence of C/T at $H = 0$ T shows no peak structure down to 2 K, presumably because the energy split of the Kramers doublet is smaller than the lowest measurable temperature of 2 K [23]. The emergence of the C/T peak at 5 K with the application of a magnetic field of 9 T can be interpreted as a manifestation of the field-induced enhancement of Zeeman splitting of the Kramers doublet from less than 2 to 5 K [see Fig. 3(b)]. On the other hand, in the rhombohedral structure phase ($x < 0.6$), the electronic specific heat coefficient γ estimated from the fits of $C/T (= \gamma + \beta T^2 + \alpha T^4)$ at high temperatures increases with increasing x (the detail on analysis is shown in Fig. S6 and Table S6, see SM [20]). In addition, the Schottky anomaly due to the Kramers doublet is almost absent, reflecting the fact that the valence of the Pr ion is close to +3. Consequently, the increase in γ as a function of x below 0.6 indicates an enhancement of the effective mass, as observed for $La_{1-x}Nd_xCuO_3$ ($x < 0.6$) [16]. As for the origin of the discontinuous jump at around $x = 0.6$, it is reasonable to consider the contribution from the Schottky anomaly.

III. DISCUSSION

In order to discuss the difference in the band structure between $LaCuO_3$ and $PrCuO_3$, we performed first-principles band calculations as shown in Figs. 4(a) and 4(b), respectively (see SM, which includes Refs. [24–32], at [20] for details of first-principles calculations). $LaCuO_3$ has three-dimensional dispersive bands near the Fermi energy. On the other hand, the bandwidth near the Fermi energy of $PrCuO_3$ is narrower than that of $LaCuO_3$, reflecting the low dimensionality and

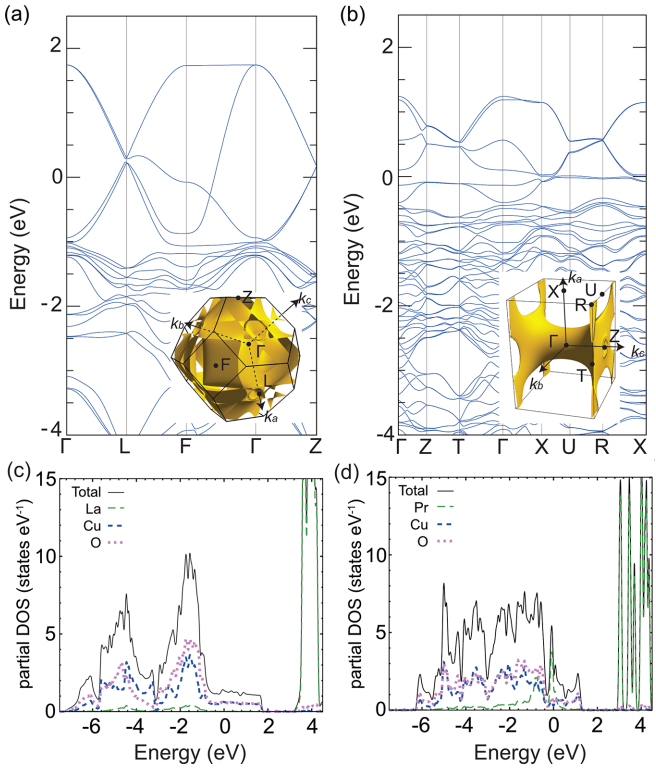

FIG. 4. The band structures for (a) $LaCuO_3$ and (b) $PrCuO_3$. Insets show the Fermi surfaces at 0.5 eV. [(c), (d)] The total density of states (black line) and the partial density of states of La/Pr orbital (green line), Cu orbital (blue line), and O orbital (red line) for (c) $LaCuO_3$ and (d) $PrCuO_3$.

the lattice distortion. Furthermore, several bands, for instance, along the Γ-X direction, exhibit almost no dispersion, forming quasi-one-dimensional Fermi surfaces, which reflects the presence of the conductive Cu-O chains along the c axis (see the inset of Fig. 4(b); for the Fermi surfaces at selected energies in Fig. S7, see SM [20]). Figures 4(c) and 4(d) depict the density of states (DOS) for $LaCuO_3$ and $PrCuO_3$, respectively. In the case of $LaCuO_3$, the DOS near the Fermi energy is small and consists mainly of Cu-d orbitals. On the other hand, $PrCuO_3$ shows a peak structure in the DOS composed of Pr-f orbitals in the vicinity of the Fermi energy, suggesting the hybridization between the Cu-d orbitals and the Pr-f orbitals, which is reminiscent of the Kondo systems [33]. Consistent with the calculation, the relatively large Pauli paramagnetism $\chi_0 = 1.2 \times 10^{-3}$ emu/mol is observed for $PrCuO_3$, which is characteristic to strongly correlated systems [34].

The band calculations largely align with the experimental results. First, the experimental results show that the Cu valence in $LaCuO_3$ is +3, while in $PrCuO_3$ it is closer to +2. The band calculations suggest that the unique divalent nature of Cu ions in $PrCuO_3$ is caused by significant hybridization of the Pr-4f and Cu-3d orbitals. The hybridization of the itinerant d-orbital and localized f orbital is reminiscent of the "Kondo hybridization" observed in so-called heavy-fermion systems. In fact, the band structure presented in Fig. 4(b) shows pseudogap structures formed by the hybridization of the Cu-d and Pr-f orbitals (see Fig. S8 in the SM [20]). The contribution of Pr-f orbitals near the Fermi energy manifests itself as the enhancement of γ by Pr doping in the rhombohedral phase. The similar orbital hybridization between A and B sites in perovskite-type oxides has been reported in $CaCu_3Ru_4O_{12}$, where Kondo hybridization occurs between the localized d orbitals of Cu^{2+} and the delocalized d orbitals of Ru^{4+}. However, the electronic properties of $CaCu_3Ru_4O_{12}$ may be rather different from those of $PrCuO_3$, as it shows metallic behavior [35,36]. Note that a one-dimensional material, such as $CeCo_2Ga_8$, also exhibits heavy-fermion behavior [37], while coherent metallic conduction is realized even at low temperatures, unlike the case of $PrCuO_3$.

As another origin of the pseudogap structure near the Fermi energy, we also consider the possible formation of the Mott-like gap due to the enhancement of electron correlation in the quasi-one-dimensional lattice with nearly divalent Cu ions. However, the intersite charge transfer is incomplete so that the Pr and Cu ions are in mixed valent states, implying that the energy gap is not fully opened, as reflected in the temperature dependence of resistivity and the optical conductivity. In any case, the emergence of the quasi-one-dimensional structure and the incoherent bands in $La_{1-x}Pr_xCuO_3$ at high x can be associated with the strong d-f hybridization and the intersite charge transfer, yielding Jahn-Teller active Cu^{2+} ions.

IV. CONCLUSION

In conclusion, we found that Pr doping on a metallic perovskite $LaCuO_3$ induces nearly localized nonmetallic state upon the structural transition to a quasi-one-dimensional perovskite phase. This transition is accompanied by significant changes in the valence states of Cu and Pr ions, as well as the electron-mass enhancement due to the hybridization between Cu 3d, O 2p, and Pr 4f orbitals. The structural and electronic transformations suggest the formation of incoherent electronic bands in the Pr-rich compounds, which are further supported by the measurements of optical conductivity and specific heat and the first-principles calculations. These findings highlight the interplay between dimensionality, charge transfer, and d-f orbital hybridization in determining the physical properties of $La_{1-x}Pr_xCuO_3$. This study offers important clues to explore novel correlated states, such as heavy-fermion states and exotic superconducting states, in low-dimensional oxides having multiple cations with charge and orbital degrees of freedom.

ACKNOWLEDGMENTS

The authors thank T. Onimaru and K. Matsuhira for useful comments. This work was partly supported by JSPS, KAKENHI (Grants No. 19H05824, No. 19K14652, No. 20H01866, No. 21K18813, No. 22H01177, No. 22H00343, No. 22J13408, No. 23H04871, and No. 24K00570), FOREST (Grant No. JPMJFR236K) and CREST (Grant No. JPMJCR2435) from JST, and the Murata Science Foundation and Asahi Glass Foundation. The synchrotron powder XRD was performed with the approvals of the Photon Factory Program Advisory Committee (Proposals No. 2018S2-006 and No. 2021S2-004).

[1] J. B. Goodenough and J.-S. Zhou, Localized to itinerant electronic transitions in transition-metal oxides with the perovskite structure, Chem. Mater. **10**, 2980 (1998).

[2] T. Kimura, T. Goto, H. Shintani, K. Ishizaka, T. Arima, and Y. Tokura, Magnetic control of ferroelectric polarization, Nature (London) **426**, 55 (2003).

[3] S. Ishiwata, Y. Kaneko, Y. Tokunaga, Y. Taguchi, T.-H. Arima, and Y. Tokura, Perovskite manganites hosting versatile multiferroic phases with symmetric and antisymmetric exchange strictions, Phys. Rev. B **81**, 100411(R) (2010).

[4] J. B. Torrance, P. Lacorre, A. I. Nazzal, E. J. Ansaldo, and C. Niedermayer, Systematic study of insulator-metal transitions in perovskites RNiO$_3$ (R = Pr,Nd,Sm,Eu) due to closing of charge-transfer gap, Phys. Rev. B **45**, 8209 (1992).

[5] J. A. Alonso, M. J. Martínez-Lope, M. T. Casais, J. L. García-Muñoz, and M. T. Fernández-Díaz, Room-temperature monoclinic distortion due to charge disproportionation in RNiO$_3$ perovskites with small rare-earth cations (R = Ho Y, Er, Tm, Yb, and Lu): A neutron diffraction study, Phys. Rev. B **61**, 1756 (2000).

[6] S. Ishiwata, M. Azuma, M. Takano, E. Nishibori, M. Takata, M. Sakata, and K. Kato, High pressure synthesis, crystal structure and physical properties of a new Ni(II) perovskite BiNiO$_3$, J. Mater. Chem. **12**, 3733 (2002).

[7] M. Azuma, S. Carlsson, J. Rodgers, M. G. Tucker, M. Tsujimoto, S. Ishiwata, S. Isoda, Y. Shimakawa, M. Takano, and J. P. Attfield, Pressure-induced intermetallic valence transition in BiNiO$_3$, J. Am. Chem. Soc. **129**, 14433 (2007).

[8] M. Azuma *et al.*, Colossal negative thermal expansion in BiNiO$_3$ induced by intermetallic charge transfer, Nat. Commun. **2**, 347 (2011).

[9] S. Ishiwata *et al.*, Pressure/temperature/substitution-induced melting of A-site charge disproportionation in Bi$_x$La$_x$NiO$_3$ ($0 \leqslant x \leqslant 0.5$), Phys. Rev. B **72**, 045104 (2005).

[10] Y. W. Long, N. Hayashi, T. Saito, M. Azuma, S. Muranaka, and Y. Shimakawa, Temperature-induced A-B intersite charge transfer in an A-site-ordered LaCu$_3$Fe$_4$O$_{12}$ perovskite, Nature (London) **458**, 60 (2009).

[11] I. Yamada *et al.*, Giant negative thermal expansion in the iron perovskite SrCu$_3$Fe$_4$O$_{12}$, Angew. Chem. Int. Ed Engl. **50**, 6579 (2011).

[12] P. H. Hor, R. L. Meng, Y. Q. Wang, L. Gao, Z. J. Huang, J. Bechtold, K. Forster, and C. W. Chu, Superconductivity above 90 K in the square-planar compound system ABa$_2$Cu$_3$O$_{6+x}$ with A = Y, La, Nd, Sm, Eu, Gd, Ho, Er and Lu, Phys. Rev. Lett. **58**, 1891 (1987).

[13] G. Demazeau, C. Parent, M. Pouchard, and P. Hagenmuller, Sur deux nouvelles phases oxygenees du cuivre trivalent: LaCuO$_3$ et La$_2$Li$_{0.50}$Cu$_{0.50}$O$_4$, Mater. Res. Bull. **7**, 913 (1972).

[14] C. Weigl and K.-J. Range, Rhombohedral LaCuO$_3$: High-pressure synthesis of single crystals and structure refinement, J. Alloys Compd. **200**, L1 (1993).

[15] J. F. Bringley, B. A. Scott, S. J. La Placa, R. F. Boehme, T. M. Shaw, M. W. McElfresh, S. S. Trail, and D. E. Cox, Synthesis of the defect perovskite series LaCuO$_{3-\delta}$ with copper valence varying from 2+ to 3+, Nature (London) **347**, 263 (1990).

[16] J.-S. Zhou, W. Archibald, and J. B. Goodenough, Approach to Curie-Weiss paramagnetism in the metallic perovskites La$_{1-x}$Nd$_x$CuO$_3$, Phys. Rev. B **61**, 3196 (2000).

[17] B.-H. Chen, D. Walker, E. Suard, B. A. Scott, B. Mercey, M. Hervieu, and B. Raveau, High pressure synthesis of NdCuO$_{3-\delta}$ perovskites ($0 \leqslant x \leqslant 0.5$), Inorg. Chem. **34**, 2077 (1995).

[18] M. Karppinen, H. Yamauchi, H. Suematsu, K. Isawa, M. Nagano, R. Itti, and O. Fukunaga, Control on the copper valence and properties by oxygen content adjustment in the LaCuO$_{3-y}$ system ($0 \leqslant y \leqslant 0.5$), J. Solid State Chem. **130**, 213 (1997).

[19] M. Ito *et al.*, High pressure synthesis of a quasi-one-dimensional GdFeO$_3$-type perovskite PrCuO$_3$ with nearly divalent Cu ions, Chem. Commun. **55**, 8931 (2019).

[20] See Supplemental Material at http://link.aps.org/supplemental/10.1103/PhysRevB.111.085153 for the experimental methods, details of first-principles calculations, details of experimental analysis, Fermi surfaces, and band structures of PrCuO$_3$ near the Fermi energy [29].

[21] K. Momma and F. Izumi, VESTA 3 for three-dimensional visualization of crystal, volumetric and morphology data, J. Appl. Crystallogr. **44**, 1272 (2011).

[22] J.-S. Zhou, L. G. Marshall, and J. B. Goodenough, Mass enhancement versus Stoner enhancement in strongly correlated metallic perovskites: LaNiO$_3$ and LaCuO$_3$, Phys. Rev. B **89**, 245138 (2014).

[23] J. Hejtmánek, E. Šantavá, K. Knížek, M. Maryško, Z. Jirák, T. Naito, H. Sasaki, and H. Fujishiro, Metal-insulator transition and the Pr^{3+}/Pr^{4+} valence shift in (Pr$_{1-y}$Y$_y$)$_{0.7}$Ca$_{0.3}$CoO$_3$, Phys. Rev. B **82**, 165107 (2010).

[24] P. Blaha, K. Schwarz, G. K. H. Madsen, D. Kvasnicka, J. Luitz, R. Laskowski, F. Tran, and L. D. Marks, *WIEN2k: An Augmented Plane Wave + Local Orbitals Program for Calculating Crystal Properties* (Karlheinz Schwarz, Vienna University of Technology, Austria, 2018).

[25] P. Blaha, K. Schwarz, F. Tran, R. Laskowski, G. K. H. Madsen, and L. D. Marks, WIEN2k: An APW+lo program for calculating the properties of solids, J. Chem. Phys. **152**, 074101 (2020).

[26] J. P. Perdew, K. Burke, and M. Ernzerhof, Generalized gradient approximation made simple, Phys. Rev. Lett. **77**, 3865 (1996).

[27] V. I. Anisimov, I. V. Solovyev, M. A. Korotin, M. T. Czyżyk, and G. A. Sawatzky, Density-functional theory and NiO photoemission spectra, Phys. Rev. B **48**, 16929 (1993).

[28] M. T. Czyżyk and G. A. Sawatzky, Local-density functional and on-site correlations: The electronic structure of La$_2$CuO$_4$ and LaCuO$_3$, Phys. Rev. B **49**, 14211 (1994).

[29] M. Kawamura, FermiSurfer: Fermi-surface viewer providing multiple representation schemes, Comput. Phys. Commun. **239**, 197 (2019).

[30] N. Marzari and D. Vanderbilt, Maximally localized generalized Wannier functions for composite energy bands, Phys. Rev. B **56**, 12847 (1997).

[31] I. Souza, N. Marzari, and D. Vanderbilt, Maximally localized Wannier functions for entangled energy bands, Phys. Rev. B **65**, 035109 (2001).

[32] G. Pizzi *et al.*, Wannier90 as a community code: New features and applications, J. Phys.: Condens. Matter **32**, 165902 (2020).

[33] F. Reinert, D. Ehm, S. Schmidt, G. Nicolay, S. Hüfner, J. Kroha, O. Trovarelli, and C. Geibel, Temperature dependence of the Kondo resonance and its satellites in CeCu$_2$Si$_2$, Phys. Rev. Lett. **87**, 106401 (2001).

[34] K. L. Holman, T. M. McQueen, A. J. Williams, T. Klimczuk, P. W. Stephens, H. W. Zandbergen, Q. Xu, F. Ronning, and

R. J. Cava, Insulator to correlated metal transition in $V_{1-x}Mo_xO_2$, Phys. Rev. B **79**, 245114 (2009).

[35] W. Kobayashi, I. Terasaki, J.-I. Takeya, I. Tsukada, and Y. Ando, A novel heavy-fermion state in $CaCu_3Ru_4O_{12}$, J. Phys. Soc. Jpn. **73**, 2373 (2004).

[36] D. Takegami *et al.*, $CaCu_3Ru_4O_{12}$: A high-Kondo-temperature transition-metal oxide, Phys. Rev. X **12**, 011017 (2022).

[37] L. Wang *et al.*, Heavy fermion behavior in the quasi-one-dimensional Kondo lattice $CeCo_2Ga_8$, npj Quantum Mater. **2**, 36 (2017).